Chemical Science

ROYAL SOCIETY OF CHEMISTRY

EDGE ARTICLE

View Article Online
View Journal | View Issue

Cite this: *Chem. Sci.*, 2025, **16**, 17859

All publication charges for this article have been paid for by the Royal Society of Chemistry

From the laboratory to space: unveiling isomeric diversity of C_5H_2 in the reaction of tricarbon (C_3, $X^1\Sigma_g^+$) with the vinyl radical (C_2H_3, X^2A')

Iakov A. Medvedkov,[a] Anatoliy A. Nikolayev,[b] Shane J. Goettl,[a] Zhenghai Yang,[a] Alexander M. Mebel *[c] and Ralf I. Kaiser *[a]

By connecting laboratory dynamics with cosmic observables, this work highlights the critical role of reactions between highly reactive species in shaping the molecular inventory of the interstellar medium and opens new windows into the spectroscopically elusive corners of astrochemical complexity. The gas phase formation of distinct C_5H_2 isomers is explored through the bimolecular reaction of tricarbon (C_3, $X^1\Sigma_g^+$) with the vinyl radical (C_2H_3, X^2A') at a collision energy of 44 ± 1 kJ mol^{-1} employing the crossed molecular beam technique augmented by electronic structure and Rice–Ramsperger–Kassel–Marcus (RRKM) calculations. This barrierless and exoergic reaction follows indirect dynamics and is initiated by the addition of tricarbon to the radical center of the vinyl radical forming a C_s symmetric doublet collisional complex ($CCCCHCH_2$). Subsequent low-barrier isomerization steps culminate in the resonantly stabilized 2,4-pentadiynyl-1 radical ($CHCCCCH_2$), which decomposes *via* atomic hydrogen loss. Statistical calculations identify linear, triplet pentadiynylidene (**p2**, $X^3\Sigma_g^-$) as the dominant product, while singlet carbenes ethynylcyclopropenylidene (**p1**, X^1A'), pentatetraenylidene (**p3**, X^1A_1), and ethynylpropadienylidene (**p4**, X^1A') are formed with lower branching ratios. The least stable isomer, 2-cyclopropen-1-ylidenethenylidene ('eiffelene'; **p5**, X^1A_1), remains thermodynamically feasible, but exhibits negligible branching ratios. Two isomers detected in TMC-1 to date (**p1** and **p3**) possess significant dipole moments making them amenable to radio telescopic observations, whereas linear pentadiynylidene (**p2**; $D_{\infty h}$) is only traceable *via* infrared spectroscopy or through its cyanopentadiynylidene derivative (HCCCCCCN). This study highlights the isomer diversity accessed in the low temperature hydrocarbon chemistry of barrierless and exoergic bimolecular reactions involving two unstable, reactants in cold molecular clouds.

Received 26th June 2025
Accepted 29th August 2025

DOI: 10.1039/d5sc04699h

rsc.li/chemical-science

Introduction

The history of carbenes – neutral divalent carbon species containing two electrons that are not shared with other atoms – commenced in 1835 as a chemical curiosity with Dumas' attempt to dehydrate methanol,[1] followed by the works of Curtius (1885)[2] and Staudinger (1912).[3] Doering (1950s)[4] and Fischer (1964)[5] introduced carbenes into the preparative organic and organometallic chemistry that lead eventually to the isolation of the crystalline carbene (1,3-di-1-adamantylimidazol-2-ylidene) in 1991.[6] However, given their inherently short lifetimes and tendency for dimerization, free carbenes still represent one of the most elusive classes of organic reactive intermediates. Withal, carbenes can transiently exist under extreme conditions, including combustion processes, the interstellar medium, and planetary atmospheres, where their high reactivity plays a crucial role in molecular mass growth process of hydrocarbons. During the combustion of hydrocarbons,[7,8] carbon chain carbenes (C_nH_2) with an odd number of carbons such as C_3H_2 or C_5H_2 (Scheme 1)[9–14] tend to dimerize making them possible transient species *en route* to polycyclic aromatic hydrocarbons (PAHs), soot, and/or fullerenes.[15]

Carbenes are also well-established in astrochemistry (Scheme 2); due to their high reactivity, they have been suggested to play a role in the hydrocarbon chemistry of cold environments like the atmosphere of Titan[16] and in cold molecular clouds such as the Taurus molecular cloud (TMC-1),[10] with cyclopropenylidene (*c*-C_3H_2) acclaimed as the first cyclic molecular species detected in interstellar molecular clouds.[17]

The recent astronomical detection of ethynylcyclopropenylidene (*c*-C_3HC_2H; **1**)[9] and pentatetraenylidene (*l*-C_5H_2; **3**)[10] has significantly increased interest in C_5H_2 isomers and their synthetic pathways within the interstellar medium (ISM)

[a]*Department of Chemistry, University of Hawai'i at Manoa, Honolulu, HI 96822, USA. E-mail: ralfk@hawaii.edu*

[b]*Samara National Research University, Samara 443086, Russia*

[c]*Department of Chemistry and Biochemistry, Florida International University, Miami, Florida 33199, USA. E-mail: mebela@fiu.edu*

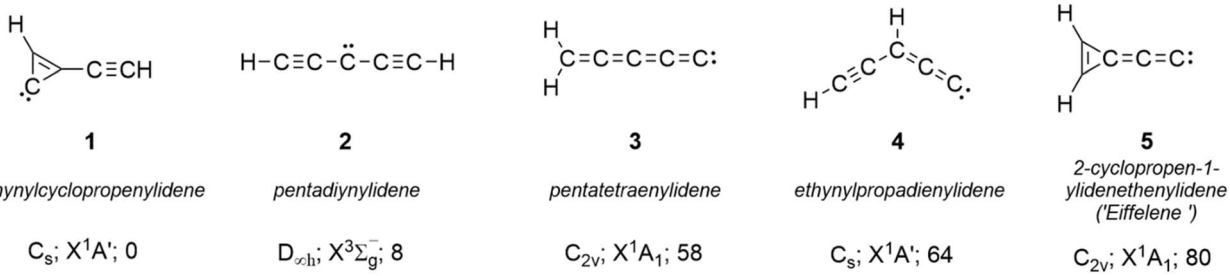

Scheme 1 Distinct C_5H_2 isomers that were detected in space (1 and 3)[9,10] and in a laboratory (1–5).[11–14] Energies were calculated at the CCSD(T)-F12/cc-pVTZ-f12//ωB97X-D/6-311G(d,p) level of theory and are shown in kJ mol^{-1}.

under molecular cloud conditions with temperatures as low as 10 K. This attention is also aligned with ongoing broader investigations into carbon-chain molecules,[18,19] which constitute approximately 40% of the currently detected species in the ISM. For carbenes H_2C_n with $n > 3$, detailed information regarding the formation of their various possible isomers remains limited. Thus, chemical networks, such as UMIST RATE12,[20] do not distinguish between C_5H_2 isomers. For example, in one of the modeling study[10] addressing the high discrepancy between the calculated and observed peak abundance of H_2C_5, the authors conclude that the more stable isomer pentadiynylidene (HC_5H; **2**) should be substantially more abundant than the carbene *l*-H_2C_5, while the model cannot predict this trend.

The most studied molecular mass growth reaction that leads to pentadiynylidene (HC_5H; **2**) and ethynylcyclopropenylidene (*c*-C_3HC_2H; **1**) – the bimolecular reaction (1) of methylidyne (CH) with diacetylene (HCCCCH) – was explored in the crossed molecular beam experiment augmented by electronic structure, statistical, and molecular dynamics calculations.[21] Alternative molecular mass growth reactions to C_5H_2 were suggested to involve reactions (2)[22] and (3);[9] however, no detailed experimental studies on these reactions were performed. In theoretical works,[23] 15 isomers of C_5H_2 were studied at the CCSDT(Q)/CBS level of theory; two of these species ((SP-4)-spiro[2.2]pent-1,4-dien-1,4-diyl and (SP-4)-spiro[2.2]pent-1,4-dien-1,5-diyl) contain a planar tetracoordinate carbon and were suggested to serve as reactive intermediates for the formation of ethynylcyclopropenylidene (*c*-C_3HC_2H; **1**).

$$CH + HCCCCH \rightarrow C_5H_2 + H \quad (1)$$

$$C + C_4H_3 \rightarrow C_5H_2 + H \quad (2)$$

$$CCH + c\text{-}C_3H_2 \rightarrow C_5H_2 + H \quad (3)$$

Here, we introduce a previously unconsidered route for the formation of C_5H_2 isomers. By integrating crossed molecular beam experiments with *ab initio* and statistical calculations, we unravel the chemical dynamics of the reaction of ground state tricarbon (C_3, $X^1\Sigma_g^+$) with the vinyl radical (C_2H_3, X^2A') (reaction (4)). Both reactants are ubiquitous in any carbon-rich chemical system.[24–27] The single collision, crossed molecular beam technique (Fig. 1) is the most suitable experimental approach to study reactions of two highly reactive species which cannot be purchased 'in a bottle', as it allows the generation of reactants in two separated beams and monitoring products before any secondary collisions or wall effects can occur. From the perspective of physical organic chemistry, this system offers a valuable framework for probing chemical reactivity, elucidating bond dissociation mechanisms, and advancing the synthesis of elusive carbenes.

$$C_3\ (36\ amu) + C_2H_3\ (27\ amu) \rightarrow C_5H_2\ (62\ amu) + H\ (1\ amu) \quad (4)$$

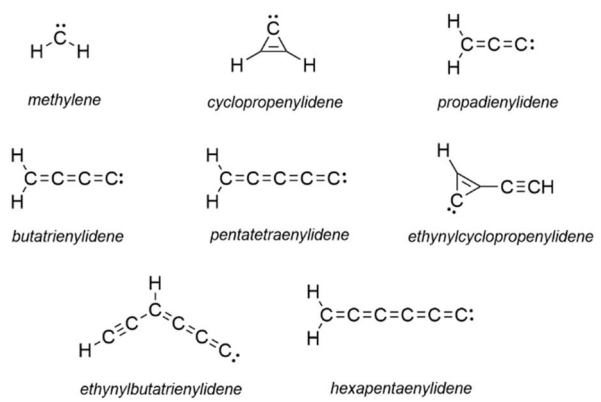

Scheme 2 Carbenes detected in the interstellar medium to date.

Results

Laboratory frame

Reactive scattering signal for the reaction of tricarbon (C_3; 36 amu) with the vinyl radical (C_2H_3; 27 amu) was observed at the mass-to-charge (m/z) ratio of $m/z = 62$ ($C_5H_2^+$) suggesting the formation of the C_5H_2 product *via* an atomic hydrogen loss channel (reaction (4)). Tricarbon molecules were generated *via* laser ablation of a rotating carbon rod, while vinyl radicals were generated *via* photodissociation of vinyl bromide; detailed experimental method is described in the SI.† Note that tricarbon molecules can also react with the non-photolyzed vinyl bromide precursor. However, (i) the center of mass angle of 69° in this system is much closer to the secondary beam and (ii)

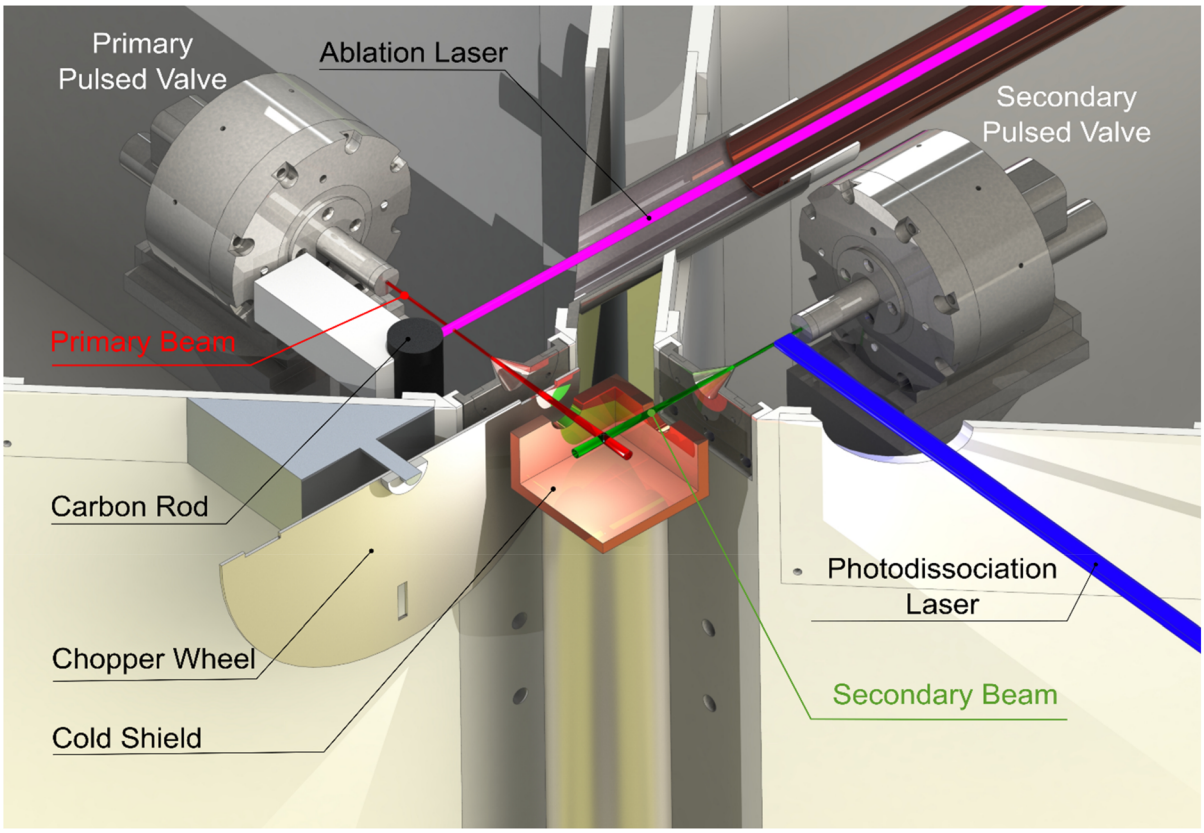

Fig. 1 Experimental setup, side view on the cross point.

recording of the $m/z = 62$ TOF at the CM angle of the tricarbon – vinyl radical system (34°) showed no detectable signal with the 193 nm excimer laser off, *i.e.* no vinyl radicals in the beam, only the vinyl bromide precursor, after the same data collection time (Fig. S2). Therefore, under our experimental conditions, tricarbon does not react with vinyl bromide. The corresponding TOF spectra of the reaction of tricarbon with the vinyl radical were collected at $m/z = 62$ and were then normalized to the signal at the CM angle to obtain the LAD (Fig. 2a). Notable features of the LAD include its width of at least 25° and symmetry around the CM angle at 34.4 ± 1.0°. These findings propose that the C_5H_2 products were formed *via* indirect scattering dynamics through complex formation involving one or more C_5H_3 intermediates.[28–30]

Center-of-mass frame

Exploiting a forward-convolution routine,[31–33] the laboratory data (TOFs, LADs) for the tricarbon – vinyl radical system were converted into the center-of-mass reference frame *via* a single channel fit (reaction (4)). The best-fit CM functions are depicted in Fig. 3. The error ranges of the $P(E_T)$ and $T(\theta)$ functions are determined within the 1σ limits of the corresponding laboratory angular distribution and beam parameters (beam spreads, beam velocities) while maintaining a good fit of the laboratory TOF spectra and LAD. The translational energy flux distribution $P(E_T)$ (Fig. 3a) encapsulates critical insights into reaction dynamics and thermodynamics. The derived $P(E_T)$ distribution exhibits a maximum translational energy release (E_{max}) of 204 ± 23 kJ mol^{-1}. Energy conservation dictates that for those molecules born without internal excitation, E_{max} is the sum of the collision energy (E_C) and the reaction energy release. Taking into account the collision energy of 44 ± 1 kJ mol^{-1}, the reaction energy was determined to be exoergic by 160 ± 24 kJ mol^{-1}. Withal, the $P(E_T)$ distribution peaks away from zero (25 ± 3 kJ mol^{-1}) indicating a tight exit transition state for at least one exit channel.[34] The average translational energy of the products was derived to be 54 ± 6 kJ mol^{-1}, suggesting that 27 ± 6% of the total available energy is channeled into the translational degrees of freedom of the products; this implies that the reaction mechanism proceeds through the formation of a covalently bound C_5H_3 intermediate (indirect scattering dynamics).[28–30]

The center-of-mass angular distribution $T(\theta)$ can provide additional information about the reaction dynamics (Fig. 3b). The tricarbon plus vinyl system reveals forward-backward symmetry with respect to 90°; this finding also suggests an indirect reaction mechanism involving long-lived C_5H_3 intermediate(s) that have a lifetime longer than their rotational period.[35] Finally, the maximum of the $T(\theta)$ at 90° highlights geometrical constraints of the decomposing complex ("sideways scattering"), revealing that the hydrogen atom is eliminated nearly perpendicularly to the plane of the decomposing complex and almost parallel to the total angular momentum vector.[34,36] Foresaid findings are also enclosed in the flux

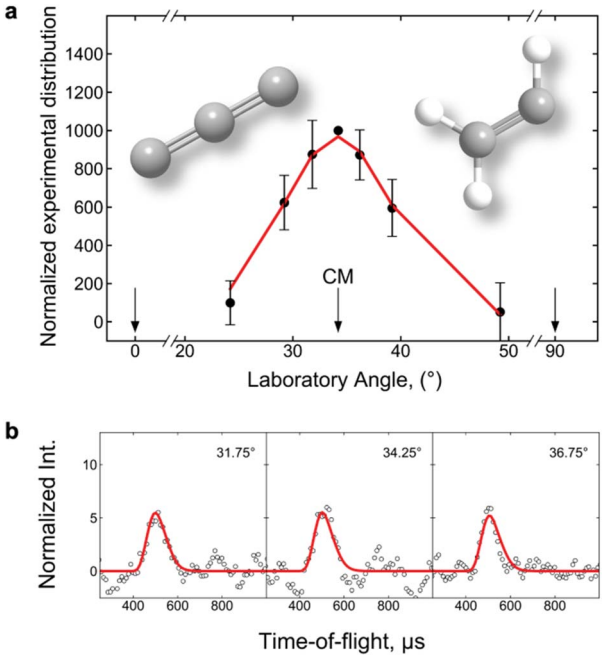

Fig. 2 (a) Laboratory angular distribution and (b) time-of-flight (TOF) spectra recorded at $m/z = 62$ for the reaction of the tricarbon (C_3; $X^1\Sigma_g^+$) with the vinyl radical (C_2H_3, X^2A') at a collision energy of 44 ± 1 kJ mol^{-1}. The circles represent the experimental data and the solid lines are the best fits.

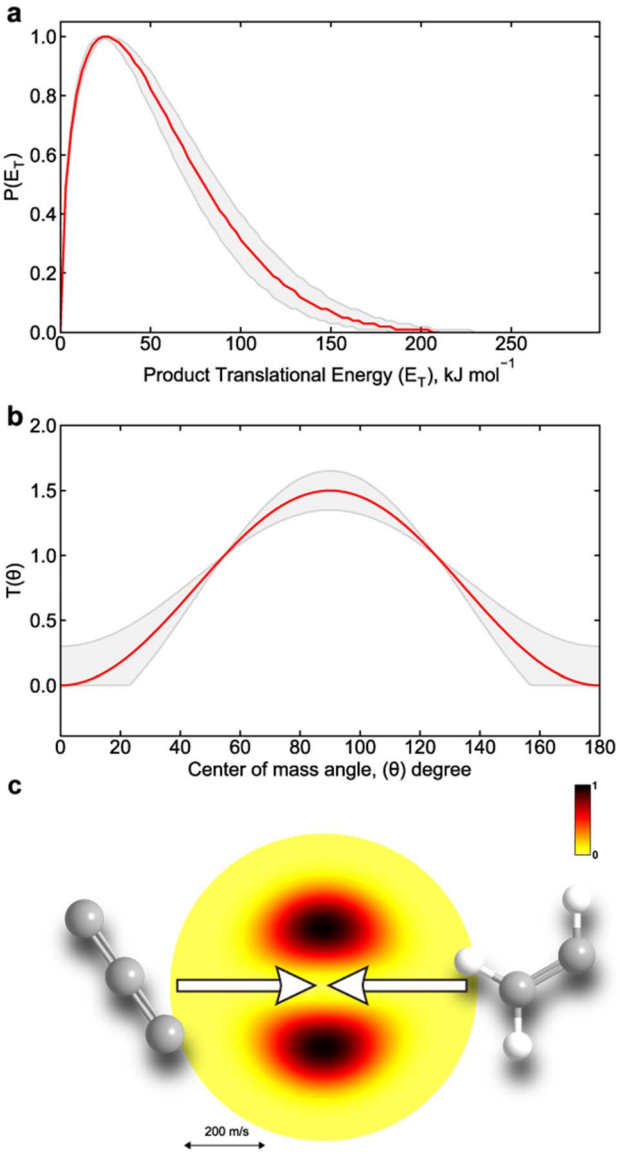

Fig. 3 (a) Center-of-mass translational energy (P(E_T)), (b) angular distributions (T(θ)), and (c) corresponding flux contour map for the reaction of the tricarbon (C_3; $X^1\Sigma_g^+$) with the vinyl radical (C_2H_3, X^2A'). For the T(θ), the direction of the C_3 beam is defined as 0° and of the C_2H_3 as 180°. Solid lines represent the best fit, while shaded areas indicate the error limits.

contour map (Fig. 3c), which depicts an overall image of the reaction scattering process.

Discussion

Now we combine our experimental results with electronic structure and statistical calculations to unlock the underlying chemical dynamics and reaction mechanism(s) of tricarbon (C_3, $X^1\Sigma_g^+$) reaction with vinyl radical (C_2H_3, X^2A') in the gas phase. The computations discovered 69 reaction intermediates leading to 46 feasible distinct products on the full potential energy surfaces (PES) (Fig. S3–S6). Structures of 43 distinct C_5H_2 isomers were considered during this study (Fig. S7). Results of Rice–Ramsperger–Kassel–Marcus (RRKM) calculations (Tables S1 and S2) are compiled in the SI. These computations (Table S1) reveal that atomic hydrogen loss channels predominate in the reaction mechanism with total branching ratios exceeding 99%. Only pathways that lead to the products with branching ratios exceeding 0.1% are discussed in the main manuscript. Detailed theoretical methods are described in the SI.

Here, the computations discovered 11 reaction intermediates (**i1–i11**) connected by 22 transition states (Fig. 4). All C_5H_2 isomers detected so far in laboratories (**p1–p5**)[11–14] and space (**p1** and **p3**)[9,10] can be formed *via* the studied mechanism. The computed relative energies of these products agree very well with the previous results.[21,23,37–39] The calculations reveal that the reaction commences with a barrierless addition of the tricarbon terminal atom without an entrance barrier to the radical center of the vinyl radical (Fig. 4) leading to only one possible collision complex **i1** stabilized by 352 kJ mol^{-1} with respect to the separated reactants. Intermediate **i1** can undergo unimolecular decomposition *via* an atomic hydrogen loss to form pentatetraenylidene (**p3**) *via* an exit channel with a barrier of about 55 kJ mol^{-1} relative to the separated products. Alternatively, **i1** can isomerize *via* two distinct [1,2]-H shifts to **i3** or **i6**; form **i2** by closing to a substituted cyclopropene ring; or undergo five-membered ring closure to **i7**. While **i6** can further undergo only the hydrogen atom elimination to **p3**, intermediates **i2** and **i3** have low-lying isomerization pathways that compete with hydrogen loss channels to **p3** (from **i3**), **p4** (from **i3**), and **p5** (from **i2**). Thus, **i2** can incorporate additional carbon in the ring accessing intermediate **i4**, which further can be

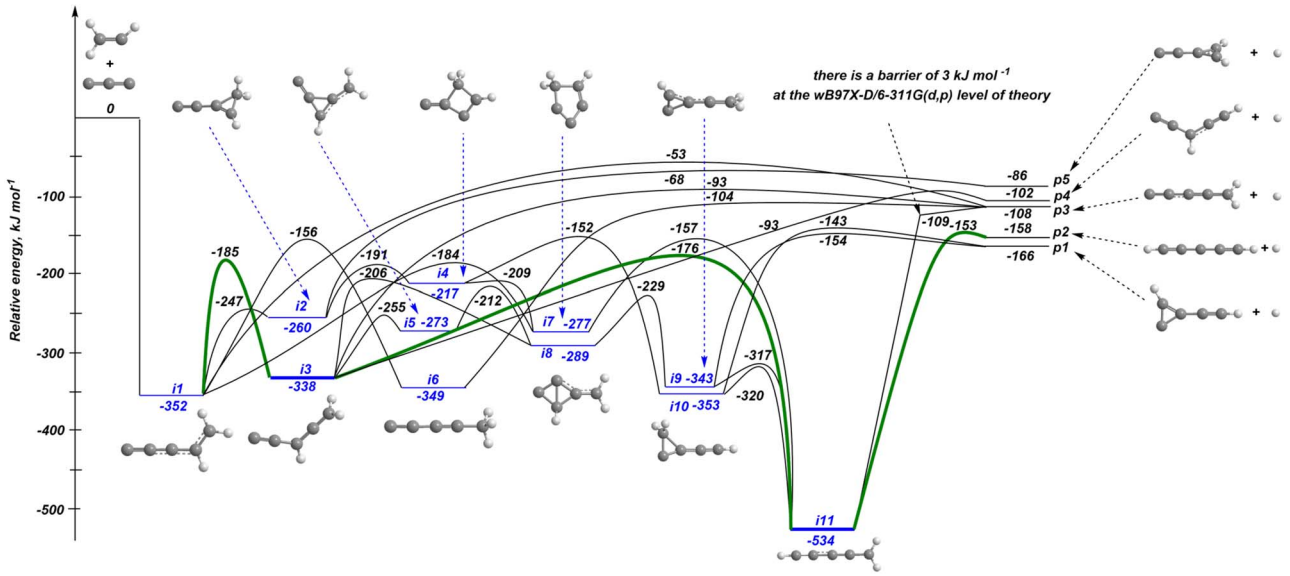

Fig. 4 Potential energy surface for the bimolecular reaction of the tricarbon (C_3; $X^1\Sigma_g^+$) with the vinyl radical (C_2H_3, X^2A') leading to C_5H_2 isomers plus atomic hydrogen calculated at the CCSD(T)-F12/cc-pVTZ-f12//ωB97X-D/6-311G(d,p) level of theory.

converted to the most stable structure on this PES – the resonantly stabilized 2,4-pentadiynyl-1 radical (**i11**; −534 kJ mol^{-1}) – *via* the **i4** → **i7** → **i11** or **i4** → **i10** → **i11** reaction pathways. The acyclic **i3** intermediate can also be converted to **i11** through the ring-closure–ring-opening reaction steps **i3** → **i5** → **i8** → **i9** → **i11** and **i3** → **i8** → **i9** → **i11** or directly in one step **i3** → **i11** *via* an activation barrier of 162 kJ mol^{-1}. Tri-membered cyclic intermediates **i9** and **i10** can only yield **p1** through atomic hydrogen loss. The resonantly stabilized C_{2v} symmetric radical **i11** provides two competing exit channels to the acyclic products pentadiynylidene (**p2**) and pentatetraenylidene (**p3**) *via* a hydrogen atom elimination with exit barriers of 381 and 425 kJ mol^{-1}, respectively.

Which of the C_5H_2 isomers dominates in this reaction? The experimentally derived reaction energy of 160 ± 24 kJ mol^{-1} for the hydrogen atom loss elimination channels nicely accounts at least for the formation of ethynylcyclopropenylidene (**p1**; −166 kJ mol^{-1}) and/or pentadiynylidene (**p2**; −158 kJ mol^{-1}) isomers under our experimental conditions *via* tight exit transition states located 5 to 23 kJ mol^{-1} above the separated products through overall indirect scattering dynamics. Thermodynamically less favorable products **p3**–**p5** might be masked in the lower energy section of the CM translational energy distribution (Fig. 3a). Note that only one loose exit transition state exists on the main PES from **i11** to **p3**. This exit transition state has a small barrier of 3 kJ mol^{-1} at the ωB97X-D/6-311G(d,p) (DFT) level of theory; however, higher-level calculations confirmed the absence of an exit barrier. The remaining transition states to products are tight meaning the reaction intermediate(s) undergo a significant reorganization of electron density rather than simple bond rupture in the unimolecular fragmentation, which is supported by our experimental findings (Fig. 3a). Additionally, the computed geometries of all exit transition states leading to **p1**–**p5** reveal that the hydrogen atom is emitted at angles ranging from 78 to 86° with respect to the rotation plane of the decomposing complexes (Fig. 5). This finding is consistent with the experimentally observed sideways scattering depicted in the T(θ) distribution (Fig. 3b).

However, while the discussed PES features align with the experimental results, they do not help to narrow down the most favorable reaction intermediates. To address this, it is beneficial to integrate our results with RRKM calculations. The statistical calculations (Table S1) determine the yield of the most thermodynamically stable isomer, ethynylcyclopropenylidene (**p1**; −166 kJ mol^{-1}) to some 10%. The most probable product is predicted to be pentadiynylidene (**p2**; −158 kJ mol^{-1}) which has an overall yield of more than 67%, while pentatetraenylidene (**p3**; −108 kJ mol^{-1}) shows lower fractions between 7 and 18%; ethynylpropadienylidene (**p4**; −102 kJ mol^{-1}) yields do not exceed 7% at collision energies from 0 to 50 kJ mol^{-1}. Although the least stable C_5H_2 isomer 2-cyclopropen-1-ylidenethenylidene ('eiffelene'; **p5**) is thermodynamically accessible (−83 kJ mol^{-1}), its branching ratios do not exceed 0.3% due to the presence of the more favorable isomerization step from intermediate **i2** to **i4** that has substantially lower barrier of 69 *versus* 192 kJ mol^{-1} for unimolecular decomposition of **i2** → **p5**.

Since the dominant product pentadiynylidene (**p2**) can only be formed from the 2,4-pentadiynyl-1 radical (**i11**), we conclude that channels including **i11** (pathways (5)–(10)) are dominant in the reaction mechanism. The low barriers (lower than those of competitive exit channels) of the isomerization reaction steps, along with the resonantly stabilized **i11** acting as an energy well at the end of these steps, determine the dominance of reaction pathways (5)–(10) in the mechanism. According to the additional RRKM calculations, which left only pathways that go through **i11** (Table S3), channel (5) exhibits the highest branching ratio, exceeding 60%, and should be the dominant

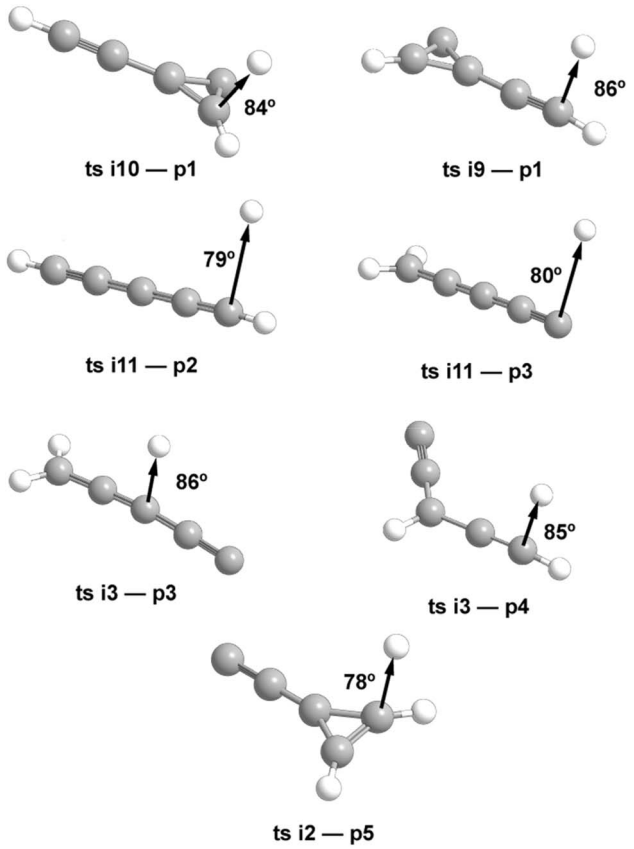

Fig. 5 Computed geometries of the exit transition states leading to the formation of C_5H_2 isomers. The angle for each departing hydrogen atom is given with respect to the rotation plane of the decomposing complex.

channel in the overall reaction mechanism. Furthermore, pathways (5), (6), and (9), which involve intermediate **i3**, collectively account for more than 90% of the total yield of intermediate **i11**. This is caused by the fact that the critical transition states on the pathways from **i2** and **i7** to **i11**, **i7–i11** (-157 kJ mol^{-1}) and **i4–i10** (-152 kJ mol^{-1}), lie higher in energy as compared to those on the pathways proceeding *via* **i3**, **i3–i11** (-176 kJ mol^{-1}), **i5–i8** (-212 kJ mol^{-1}), and **i3–i8** (-206 kJ mol^{-1}). Although the short channel (5) has a higher energy for the critical transition state than the channels (6) and (9), (5) appears to prevail due to its entropic preference resulting in a higher overall rate constant.

$$\mathbf{i1} \rightarrow \mathbf{i3} \rightarrow \mathbf{i11} \quad (5)$$

$$\mathbf{i1} \rightarrow \mathbf{i3} \rightarrow \mathbf{i5} \rightarrow \mathbf{i8} \rightarrow \mathbf{i9} \rightarrow \mathbf{i11} \quad (6)$$

$$\mathbf{i1} \rightarrow \mathbf{i2} \rightarrow \mathbf{i4} \rightarrow \mathbf{i7} \rightarrow \mathbf{i11} \quad (7)$$

$$\mathbf{i1} \rightarrow \mathbf{i7} \rightarrow \mathbf{i11} \quad (8)$$

$$\mathbf{i1} \rightarrow \mathbf{i3} \rightarrow \mathbf{i8} \rightarrow \mathbf{i9} \rightarrow \mathbf{i11} \quad (9)$$

$$\mathbf{i1} \rightarrow \mathbf{i2} \rightarrow \mathbf{i4} \rightarrow \mathbf{i10} \rightarrow \mathbf{i11} \quad (10)$$

To the best of our knowledge, only one reaction of tricarbon with a highly unstable species (carbene) has been investigated before in crossed molecular beam experiments augmented with *ab initio* calculations, namely, bimolecular barrierless C_3 plus *c*-C_3H_2 (cyclopropenylidene) $\rightarrow$*l*-C_6H + H.[40] In this study, C_3 and *c*-C_3H_2 were generated alongside various carbonaceous species (C_3H, C_4, C_4H, and C_4H_2) by a plasma discharge of 1% acetylene in He.

Conclusion

Exploiting the crossed molecular beam technique, we studied the reaction of the tricarbon (C_3, $X^1\Sigma_g^+$) reaction with the vinyl radical (C_2H_3, X^2A') at a collision energy of 44 $\pm$ 1 kJ mol^{-1}. Experimental data were augmented by electronic structure (CCSD(T)-F12/cc-pVTZ-f12//ωB97X-D/6-311G(d,p)) and RRKM calculations to elucidate the reaction mechanism. All detected to date in laboratories (**p1–p5**)[11–14] and in space (**p1** and **p3**)[9,10] C_5H_2 isomers can be formed *via* the studied mechanism. The overall barrierless and exoergic reaction involves indirect reaction dynamics. It starts with the addition of tricarbon by the terminal atom to the radical center of the vinyl radical, forming only one initial collisional complex, **i1**. The subsequent reaction dynamics is predominantly driven by low-barrier isomerization steps that ultimately lead to the resonantly stabilized 2,4-pentadiynyl-1 radical (**i11**) prior to unimolecular decomposition *via* atomic hydrogen loss. Statistical calculation identifies triplet pentadiynylidene carbene (**p2**, $X^3\Sigma_g^-$) as a primary product in this reaction, with singlet carbenes ethynylcyclopropenylidene (**p1**, X^1A'), pentatetraenylidene (**p3**; X^1A_1), and ethynylpropadienylidene (**p4**; X^1A') showing lower fractions of between 7 and 18%. The least stable thermodynamically accessible C_5H_2 isomer, 2-cyclopropen-1-ylidenethenylidene ('eiffelene'; **p5**; X^1A_1), -83 kJ mol^{-1} relative to the separated reactants, has its branching ratios below 0.3% due to the more favorable isomerization step competing with an exit channel.

The C_5H_3 potential energy surface plays an important role in combustion chemistry, governing key reaction pathways, where sequential interactions between C_5H_3 isomers and methyl radicals (CH_3) yield various C_6H_6 isomers,[41–43] including benzene – the fundamental precursor to polycyclic aromatic hydrocarbons (PAHs). We would like to highlight that two of the isomers, ethynylcyclopropenylidene (*c*-C_3HC_2H, **p1**) and pentatetraenylidene (*l*-C_5H_2, **p3**), were detected in the TMC-1 (ref. 9 and 10) by radio telescopes, and they also hold prominent branching ratios in the title reaction. Both of them exhibit sizeable dipole moments of 3.52 (C_s; **p1**) and 5.81 D (C_{2v}; **p3**), while the dominant high-symmetric pentadiynylidene (HCCCCCH; $D_{\infty h}$; **p2**) carbene lacks a permanent dipole moment and, therefore, is invisible for the rotational spectroscopy and can only be traced in deep space through infrared spectroscopy. Perhaps, the recently proposed search with the focus on the carbon-chain species,[19] utilizing the James Webb Space Telescope (JWST; infrared spectroscopy) will drag to light the missing C_5H_2 isomer.

Author contributions

Supervision and funding acquisition – R. I. K. and A. M. M; formal analysis – I. A. M.; investigation – I. A. M., S. J. G. and Z. Y. carried out the experimental measurements, A. A. N. – carried out the theoretical analysis; writing original draft – I. A. M.; writing – review & editing – I. A. M, R. I. K., A. M. M, A. A. N.

Conflicts of interest

There are no conflicts to declare.

Data availability

The data supporting the findings of this study are available within the article and the SI. Supplementary information: The supplemental material contains details of the experimental and theoretical methods, full potential energy surface, results of the RRKM calculations, optimized Cartesian coordinates (Å) and vibrational frequencies (cm^{-1}) for all intermediates, transition states, reactants, and products involved in the C_3 + C_2H_3 reaction. The authors have cited additional references within the SI.[44–72]

Acknowledgements

The experimental studies at the University of Hawai'i at Manoa were supported by the US Department of Energy, Basic Energy Sciences (DE-FG02-03ER15411).

References

1 J. B. Dumas and E. Piligot, *Ann. Chim. Phys.*, 1835, **58**, 5.
2 E. Buchner and Th. Curtius, *Ber. Dtsch. Chem. Ges.*, 1885, **18**, 2377–2379.
3 H. Staudinger and O. Kupfer, *Ber. Dtsch. Chem. Ges.*, 1912, **45**, 501–509.
4 W. von E. Doering and A. K. Hoffmann, *J. Am. Chem. Soc.*, 1954, **76**, 6162–6165.
5 E. O. Fischer and A. Maasböl, *Angew. Chem., Int. Ed. Engl.*, 1964, **3**, 580–581.
6 A. J. I. Arduengo, R. L. Harlow and M. Kline, *J. Am. Chem. Soc.*, 1991, **113**, 361–363.
7 W. Boullart, K. Devriendt, R. Borms and J. Peeters, *J. Phys. Chem.*, 1996, **100**, 998–1007.
8 C. A. Taatjes, S. J. Klippenstein, N. Hansen, J. A. Miller, T. A. Cool, J. Wang, M. E. Law and P. R. Westmoreland, *Phys. Chem. Chem. Phys.*, 2005, **7**, 806–813.
9 J. Cernicharo, M. Agúndez, C. Cabezas, B. Tercero, N. Marcelino, J. R. Pardo and P. de Vicente, *Astron. Astrophys.*, 2021, **649**, L15.
10 C. Cabezas, B. Tercero, M. Agúndez, N. Marcelino, J. R. Pardo, P. de Vicente and J. Cernicharo, *Astron. Astrophys.*, 2021, **650**, L9.
11 C. A. Gottlieb, M. C. McCarthy, V. D. Gordon, J. M. Chakan, A. J. Apponi and P. Thaddeus, *Astrophys. J.*, 1998, **509**, L141.
12 M. C. McCarthy, M. J. Travers, A. Kovács, W. Chen, S. E. Novick, C. A. Gottlieb and P. Thaddeus, *Science*, 1997, **275**, 518–520.
13 M. J. Travers, M. C. McCarthy, C. A. Gottlieb and P. Thaddeus, *Astrophys. J.*, 1997, **483**, L135.
14 J. Fulara, P. Freivogel, D. Forney and J. P. Maier, *J. Chem. Phys.*, 1995, **103**, 8805–8810.
15 N. S. Goroff, *Acc. Chem. Res.*, 1996, **29**, 77–83.
16 E. Hébrard, M. Dobrijevic, Y. Bénilan and F. Raulin, *J. Photochem. Photobiol., C*, 2006, **7**, 211–230.
17 P. Thaddeus, J. M. Vrtilek and C. A. Gottlieb, *Astrophys. J.*, 1985, **299**, L63.
18 K. Taniguchi, P. Gorai and J. C. Tan, *Astrophys. Space Sci.*, 2024, **369**, 34.
19 K. Taniguchi, R. M. Lau and M. Saito, *Life Sci. Space Res.*, 2025, DOI: **10.1016/j.lssr.2025.05.002**.
20 T. J. Millar, C. Walsh, M. V. de Sande and A. J. Markwick, *Astron. Astrophys.*, 2024, **682**, A109.
21 C. He, G. R. Galimova, Y. Luo, L. Zhao, A. K. Eckhardt, R. Sun, A. M. Mebel and R. I. Kaiser, *Proc. Natl. Acad. Sci. U. S. A.*, 2020, **117**, 30142–30150.
22 I. W. M. Smith, E. Herbst and Q. Chang, *Mon. Not. R. Astron. Soc.*, 2004, **350**, 323–330.
23 A. Karton and V. S. Thimmakondu, *J. Phys. Chem. A*, 2022, **126**, 2561–2568.
24 W. Tsang and R. F. Hampson, *J. Phys. Chem. Ref. Data*, 1986, **15**, 1087–1279.
25 X. Gu, Y. Guo, A. M. Mebel and R. I. Kaiser, *Chem. Phys. Lett.*, 2007, **449**, 44–52.
26 Y. Guo, X. Gu, F. Zhang, A. M. Mebel and R. I. Kaiser, *Phys. Chem. Chem. Phys.*, 2007, **9**, 1972–1979.
27 A. M. Mebel and R. I. Kaiser, *Int. Rev. Phys. Chem.*, 2015, **34**, 461–514.
28 R. I. Kaiser, *Chem. Rev.*, 2002, **102**, 1309–1358.
29 R. I. Kaiser, P. Maksyutenko, C. Ennis, F. Zhang, X. Gu, S. P. Krishtal, A. M. Mebel, O. Kostko and M. Ahmed, *Faraday Discuss.*, 2010, **147**, 429–478.
30 R. I. Kaiser and A. M. Mebel, *Chem. Soc. Rev.*, 2012, **41**, 5490.
31 M. F. Vernon, PhD Dissertation, University of California, 1983.
32 P. S. Weiss, PhD Dissertation, University of California, 1986.
33 R. I. Kaiser, C. Ochsenfeld, D. Stranges, M. Head-Gordon and Y. T. Lee, *Faraday Discuss.*, 1998, **109**, 183–204.
34 R. D. Levine, *Molecular reaction dynamics*, Cambridge University Press, Cambridge, UK, 2005.
35 R. D. Levine, *Molecular reaction dynamics*, Cambridge University Press, Cambridge, Paperback edn, 2009.
36 W. B. Miller, S. A. Safron and D. R. Herschbach, *Discuss. Faraday Soc.*, 1967, **44**, 108.
37 R. A. Seburg, R. J. McMahon, J. F. Stanton and J. Gauss, *J. Am. Chem. Soc.*, 1997, **119**, 10838–10845.
38 D. L. Cooper and S. C. Murphy, *Astrophys. J.*, 1988, **333**, 482.
39 Q. Fan and G. V. Pfeiffer, *Chem. Phys. Lett.*, 1989, **162**, 472–478.
40 Y.-L. Sun, W.-J. Huang and S.-H. Lee, *J. Chem. Phys.*, 2024, **160**, 044303.

41 A. M. Mebel, S. H. Lin, X. M. Yang and Y. T. Lee, *J. Phys. Chem. A*, 1997, **101**, 6781–6789.
42 C. J. Pope and J. A. Miller, *Proc. Combust. Inst.*, 2000, **28**, 1519–1527.
43 M. S. Skjøth-Rasmussen, P. Glarborg, M. Østberg, M. B. Larsen, S. W. Sørensen, J. E. Johnsson, A. D. Jensen and T. S. Christensen, *Proc. Combust. Inst.*, 2002, **29**, 1329–1336.
44 C. He, L. Zhao, A. M. Thomas, A. N. Morozov, A. M. Mebel and R. I. Kaiser, *J. Phys. Chem. A*, 2019, **123**, 5446–5462.
45 V. V. Kislov, T. L. Nguyen, A. M. Mebel, S. H. Lin and S. C. Smith, *J. Chem. Phys.*, 2004, **120**, 7008–7017.
46 A. M. Thomas, L. Zhao, C. He, A. M. Mebel and R. I. Kaiser, *J. Phys. Chem. A*, 2018, **122**, 6663–6672.
47 A. M. Thomas, C. He, L. Zhao, G. R. Galimova, A. M. Mebel and R. I. Kaiser, *J. Phys. Chem. A*, 2019, **123**, 4104–4118.
48 A. M. Thomas, S. Doddipatla, R. I. Kaiser, G. R. Galimova and A. M. Mebel, *Sci. Rep.*, 2019, **9**, 17595.
49 Y. Guo, X. Gu, E. Kawamura and R. I. Kaiser, *Rev. Sci. Instrum.*, 2006, **77**, 034701.
50 A. V. Wilson, D. S. N. Parker, F. Zhang and R. I. Kaiser, *Phys. Chem. Chem. Phys.*, 2012, **14**, 477–481.
51 N. R. Daly, *Rev. Sci. Instrum.*, 1960, **31**, 264–267.
52 J.-D. Chai and M. Head-Gordon, *Phys. Chem. Chem. Phys.*, 2008, **10**, 6615–6620.
53 R. Krishnan, J. S. Binkley, R. Seeger and J. A. Pople, *J. Chem. Phys.*, 1980, **72**, 650–654.
54 M. J. Frisch, G. W. Trucks, H. B. Schlegel, G. E. Scuseria, M. A. Robb, J. R. Cheeseman, G. Scalmani, V. Barone, B. Mennucci, G. A. Petersson, H. Nakatsuji, M. Caricato, X. Li, H. P. Hratchian, A. F. Izmaylov, J. Bloino, G. Zheng, J. L. Sonnenberg, M. Hada, M. Ehara, K. Toyota, R. Fukuda, J. Hasegawa, M. Ishida, T. Nakajima, Y. Honda, O. Kitao, H. Nakai, T. Vreven, J. A. Montgomery, J. E. Peralta, F. Ogliaro, M. Bearpark, J. J. Heyd, E. Brothers, K. N. Kudin, V. N. Staroverov, R. Kobayashi, J. Normand, K. Raghavachari, A. Rendell, J. C. Burant, S. S. Iyengar, J. Tomasi, M. Cossi, N. Rega, J. M. Millam, M. Klene, J. E. Knox, J. B. Cross, V. Bakken, C. Adamo, J. Jaramillo, R. Gomperts, R. E. Stratmann, O. Yazyev, A. J. Austin, R. Cammi, C. Pomelli, J. W. Ochterski, R. L. Martin, K. Morokuma, V. G. Zakrzewski, G. A. Voth, P. Salvador, J. J. Dannenberg, S. Dapprich, A. D. Daniels, Ö. Farkas, J. B. Foresman, J. V. Ortiz, J. Cioslowski and D. J. Fox, *Gaussian 09 (version A.1) Gaussian*, Gaussian Inc., Wallingford, CT 2009.
55 H. P. Hratchian and H. B. Schlegel, *J. Chem. Phys.*, 2004, **120**, 9918–9924.
56 T. B. Adler, G. Knizia and H.-J. Werner, *J. Chem. Phys.*, 2007, **127**, 221106.
57 G. Knizia, T. B. Adler and H.-J. Werner, *J. Chem. Phys.*, 2009, **130**, 054104.
58 T. H. Dunning Jr., *J. Chem. Phys.*, 1989, **90**, 1007–1023.
59 H.-J. Werner, P. J. Knowles, R. Lindh, F. R. Manby, M. Schütz, P. Celani, T. Korona, G. Rauhut, R. D. Amos and A. Bernhardsson, *MOLPRO (version 2015.1, A Package of Ab Initio Programs) University of Cardiff*, Cardiff, UK 2015.
60 P. Celani and H.-J. Werner, *J. Chem. Phys.*, 2000, **112**, 5546–5557.
61 T. Shiozaki, W. Győrffy, P. Celani and H.-J. Werner, *J. Chem. Phys.*, 2011, **135**, 081106.
62 J. M. L. Martin and O. Uzan, *Chem. Phys. Lett.*, 1998, **282**, 16–24.
63 H. Werner and P. J. Knowles, *J. Chem. Phys.*, 1985, **82**, 5053–5063.
64 P. J. Knowles and H.-J. Werner, *Chem. Phys. Lett.*, 1985, **115**, 259–267.
65 J. A. Miller, S. J. Klippenstein, Y. Georgievskii, L. B. Harding, W. D. Allen and A. C. Simmonett, *J. Phys. Chem. A*, 2010, **114**, 4881–4890.
66 A. Matsugi and A. Miyoshi, *Int. J. Chem. Kinet.*, 2012, **44**, 206–218.
67 J. Zhang and E. F. Valeev, *J. Chem. Theory Comput.*, 2012, **8**, 3175–3186.
68 H. Eyring, S. H. Lin and S. M. Lin, *Basic Chemical Kinetics*, John Wiley and Sons, New York, 1980.
69 J. I. Steinfeld, J. S. Francisco and W. L. Hase, *Chemical Kinetics and Dynamics*, Pearson, Upper Saddle River, N.J, 2nd edn, 1998.
70 P. J. Robinson and K. A. Holbrook, *Unimolecular Reactions*, John Wiley and Sons, New York, 1972.
71 X. Gu, Y. Guo, E. Kawamura and R. I. Kaiser, *JVST A*, 2006, **24**, 505–511.
72 I. A. Medvedkov, A. A. Nikolayev, S. J. Goettl, Z. Yang, A. M. Mebel and R. I. Kaiser, *Phys. Chem. Chem. Phys.*, 2024, **26**, 27763–27771.